# Mössbauer and X-ray Studies of Phase Composition of Fly Ashes Formed after Combustion of Ekibastuz Coal (Kazakhstan)

**Adilkhan Shokanov** [1,*]**, Mikhail Vereshchak** [2] **and Irina Manakova** [2,*]

[1] Institute of Mathematics, Physics and Informatics, Abai Kazakh National Pedagogical University, Dostyk Av. 13, Almaty 050010, Kazakhstan

[2] Institute of Nuclear Physics, Ibragimov st. 1, Almaty 050032, Kazakhstan; mikhail.vereshchak@mail.ru

[*] Correspondence: adilhan.shokanov@mail.ru (A.S.); i.manakova25@mail.ru (I.M.);
   Tel.: +7-701-735-5925 (A.S.); +7-777-172-1672 (I.M.)

check for updates

**Abstract:** Mössbauer spectroscopy and X-ray diffraction have been used to study samples of fly ashes formed after combustion of coal from the Ekibastuz basin at the thermal power plants TPP-2 and TPP-3 in Almaty (Kazakhstan). It has been established that the fractions of fly ashes contain iron in the form of magnetite $Fe_3O_4$ and hematite $\alpha$-$Fe_2O_3$. The mixed valence of iron $Fe^{3+} \leftrightarrow Fe^{2+}$ in the octahedral sublattice of magnetite is destroyed by isostructural substitution impurities. Maghemite $\gamma$-$Fe_2O_3$ is additionally present in the fly ash of TPP-3 as a product of magnetite slow oxidation. It was shown that at $T \geq 1400\,°C$ the proportion of magnetite in fly ashes increases due to decomposition of hematite, maghemite, hercynite and the drop of iron content in mullite. It was concluded that the amount of iron in magnetite is a temperature indicator of fly ashes formation. The parameters of hyperfine interactions have been determined in the iron-containing minerals of fly ashes. It was identified that formation of the fly ashes structure occurs in oxidizing atmosphere, since no traces were revealed of reducing environment effect on the phase composition.

**Keywords:** fly ash; Mössbauer spectroscopy; x-ray diffraction

## 1. Introduction

Kazakhstan is the country with the huge hydrocarbon reserves, which have a significant impact on the formation and state of the global power market. About 80% of Kazakhstan's energy supply comes from the use of solid fuel–coal. The main source of fuel for thermal power plants (TPP) is the Ekibastuz coal basin. Coal from this deposit is relatively cheap, but it is characterized by a high ash content of 50% [1,2].

Ash is formed from the mineral part of the fuel after its complete combustion and precipitates from the combustion gases by the ash collecting devices; it is finely dispersed material with $\leq 0.16$ mm grains. Currently, a huge amount of ash and slag mixture has been accumulated in the ash dumps of Kazakhstan, which creates a great threat to the environment and human health. Fly ashes of TPP plants are widely used as a raw material for industry [3–6]. Today in Kazakhstan less than 1.9 million tons of ash-slag waste is processed, which is 8% of its annual output. Low level of fly ashes application is explained, in particular, by the fact that they are heterogeneous and have a complex mineral and chemical composition. Chemical composition of fly ash of Ekibastuz coal is indicated in many papers, in particular, in [4], the content of the main components is as follows: $SiO_2$—61.5%, $Al_2O_3$—27.4%, $Fe_2O_3$—5.65%, $TiO_2$—1.49%, $CaO$—1.17%, $MgO$—0.49%, $K_2O$—0.42%, $Na_2O$—0.32%, $P_2O_5$—0.52, $MnO_2$—0.17 and $SO_3$—0.57.

Many papers have been devoted to the study of fly ashes. It has been shown in [7–12] that the main magnetic components of fly ashes are magnetite $Fe_3O_4$ and hematite $\alpha$-$Fe_2O_3$. The presence of maghemite $\gamma$-$Fe_2O_3$ in fly ash was detected in [11,13]. It is known that fly ashes contain minerals such as hercynite [13] and mullite [14], as well as silicate glasses in the form of quartz and various calcium silicates with the impurities of iron. However, in contrast to [13], the presence of hercynite in fly ash was not found in [5,14]. Despite the fairly extensive research, the detailed interpretation of the physical–chemical properties of fly ashes is still missing. In many of these studies, the Mössbauer spectroscopy, as a unique method for studying the phase composition of iron-containing phases, has not been used quite effectively. The mineral composition and properties of the ash-and-slag waste are directly related to the geological origin of the original coal, as well as to other several factors [11,15,16] determined by the technical features of certain power plants. Therefore, we should always consider local technological processing of the ash-and-slag waste in a particular region and even in a particular fuel plant.

The purpose of this paper is to study the fly ashes generated upon the combustion of the Ekibastuz coal at TPP-2 and TPP-3 in Almaty, identification of common patterns and individual characteristics of mineral components formation of fly ashes, their phase composition and dependence on the technological parameters of the furnace units.

## 2. Materials and Methods

Coal samples (Ekibastuz, Kazakhstan) from the Ekibastuz coal basin and fly ashes FA1 and FA2, produced by its combustion at the Almaty thermal power plants TPP-2 and TPP-3, respectively, were studied. TPP-2 is equipped with 8 power boilers BKZ-420-140 (Barnaul Boiler Plant, Barnaul, Russia) with a temperature in the torch core of 1500–1920 °C. TPP-3 is equipped with 6 boilers BKZ-160-100 (Barnaul Boiler Plant, Barnaul, Russia) with a temperature in the torch core of 1400–1500 °C. The powdered highly reactive substance is obtained as a result of the preliminary preparation of the fuel, which is actively ignited when it is mixed with air in the boiler furnace. Primary air is supplied through the burners at a rate of 25–30 m/s; secondary air is supplied at a rate of 40–60 m/s. Fine particles of coal combustion products were removed from the filters of the flue gas cleaning system and the samples were prepared for investigations by the methods of Mössbauer spectroscopy (MS) and X-ray diffraction (XRD). In some cases, fly ash was divided into magnetic and non-magnetic fractions. The method of magnetic separation was used for this purpose.

For the MS investigations the samples of fly ashes were mixed with paraffin at a rate of 100 mg/cm$^2$ and pressed into tablets. The Mössbauer spectra of the samples were recorded in the transmission geometry. The source of $\gamma$-radiation was $^{57}$Co in the chromium matrix. The spectra were recorded at 300 K on a nuclear gamma-resonance spectrometer MS1104Em (Research Institute of Southern Federal University, Rostov-on-Don, Russia). The reference sample $\alpha$-Fe was used for spectra calibration. The Mössbauer spectra were processed using the software SpectrRelax (Version 2.4, Lomonosov Moscow State University, Moscow, Russia) by the methods of model fitting and restoration of distributions of hyperfine parameters [17]. This program is characterized by unique capabilities in the study of locally heterogeneous systems, such as fly ash.

The X-ray diffraction studies were performed on a diffractometer D8 Advance (Bruker AXS GmbH, Karlsruhe, Germany) with copper radiation $\lambda_{\kappa\alpha}$ = 0.154051 nm and the graphite reflector. The powder X-ray files ASTM and 7CPDS were used to identify the phases.

## 3. Results

### 3.1. Mössbauer Spectroscopy

Mössbauer spectroscopy at $^{57}$Fe nuclei is the best method for detecting the iron-containing compounds and determination of the chemical state, electronic and magnetic structure of iron in them [18–21]. The MS spectrum of the Ekibastuz coal sample consists of two doublets (Figure 1). In

terms of hyperfine interactions parameters ($\delta$-isomer shift; $\varepsilon$-quadrupole shift) the first of them (the predominant one) belongs to the bivalent iron $Fe^{2+}$ in the crystal structure of iron carbonate–siderite $FeCO_3$ ($\delta = 1.230 \pm 0.005$ mm/s, $\varepsilon = 0.888 \pm 0.005$ mm/s). The remaining part of the experimental curve (13% $\pm$ 1%) is well interpreted via Mössbauer parameters of the trivalent iron $Fe^{3+}$ in the crystal structure of iron sulfide–pyrite $FeS_2$ ($\delta = 0.286 \pm 0.008$ mm/s, $\varepsilon = 0.307 \pm 0.008$ mm/s).
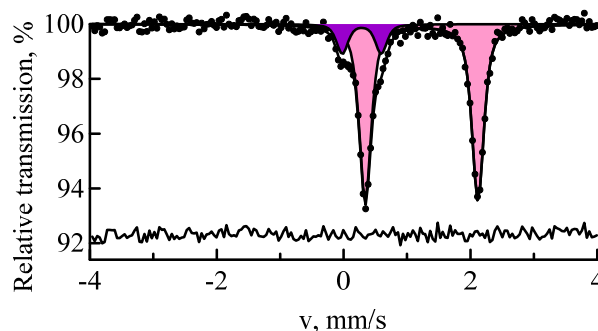


**Figure 1.** MS spectrum of $^{57}Fe$ nuclei of the Ekibastuz coal sample: siderite (pink); pyrite (purple).

Figure 2a,b shows the MS spectra and distributions of the hyperfine fields for the samples of fly ashes FA1 and FA2 respectively. Table 1 shows the Mössbauer parameters of the magnetic part of spectrum of the fly ash FA1 and their interpretation. As can be seen, the spectra have a rather complicated structure. The iron atoms occupy several positions in magnetically ordered and paramagnetic states. Therefore, for processing of the experimental data, the methods of model interpretation and restoration of distributions of hyperfine parameters of the Mössbauer spectra were used. The MS spectrum of the magnetic part of the ash FA1 is represented by a sextet with a hyperfine magnetic field of 512 kOe (H1) and distributions of the hyperfine magnetic fields of $^{57}Fe$ in the intervals of 470–510 (H2) and 350–480 kOe (H3–H7). Both distributions of P(H) were carried out by representing one Mössbauer phase. Subsequent calculation of the hyperfine parameters with approximation of the spectra by the Lorentzian shape of the spectral lines was not carried out. Data presented in Tables 1 and 2 were obtained from the analysis of the areas under the maxima of the distribution function of hyperfine magnetic fields. Due to heterogeneity of the local environment of the Mössbauer absorber nuclei, the shape of the resonance line was described by the PseudoVoigt function:

$$Z_{PV}(v) = (1 - \alpha) Z_L(v) + \alpha Z_G(v),$$

where $Z_L(v)$ is the Lorentz function and $Z_G(v)$ is the Gaussian function.

Table 1 shows that the main component of fly ash FA1 is magnetite $Fe_3O_4$. This mineral has a spinel structure. In the stoichiometric magnetite, iron is in two crystallographically non-equivalent positions: tetrahedral (A) and octahedral (B) [22]. The spectrum of pure magnetite $[Fe^{3+}]^{tetra}[Fe^{2+}, Fe^{3+}]^{octa}O_4$ consists of only two sextets with the hyperfine magnetic fields 490 and 460 kOe, representing 1/3 and 2/3 of the entire area of magnetite spectrum, respectively; i.e., S(A)/S(B) = 0.5. The first sextet corresponds to $Fe^{3+}$ cations with oxygen atoms in the tetrahedral environment, and the second sextet corresponds to $Fe^{2+}$ and $Fe^{3+}$ cations in the octahedral environment. In this case, the octahedral node can be assumed to be occupied by $Fe^{2.5+}$ cations. The analysis of the spectrum of ash FA1 shows that the sextet H1 has the parameters inherent to hematite $\alpha$-$Fe_2O_3$. The sextet H2 is specified by the $Fe^{3+}$ ions in the tetrahedral position of $Fe_3O_4$. The sextet H3 corresponds to the $Fe^{3+}$ ions and the sextets H4–H7 correspond to the $Fe^{2+}$ ions in the octahedral position of $Fe_3O_4$. The presence of two types of sextets H3 and H4–H7 is associated with the significant non-stoichiometry of magnetite. The occupancy ratio for the positions S(A)/S(B) = 0.44 $\pm$ 0.05, which is somewhat less than in the case of stoichiometric magnetite. This may be caused by the presence of some magnetically ordered phase in the fly ash, for example, magnesioferrite $MgFe_2O_4$.
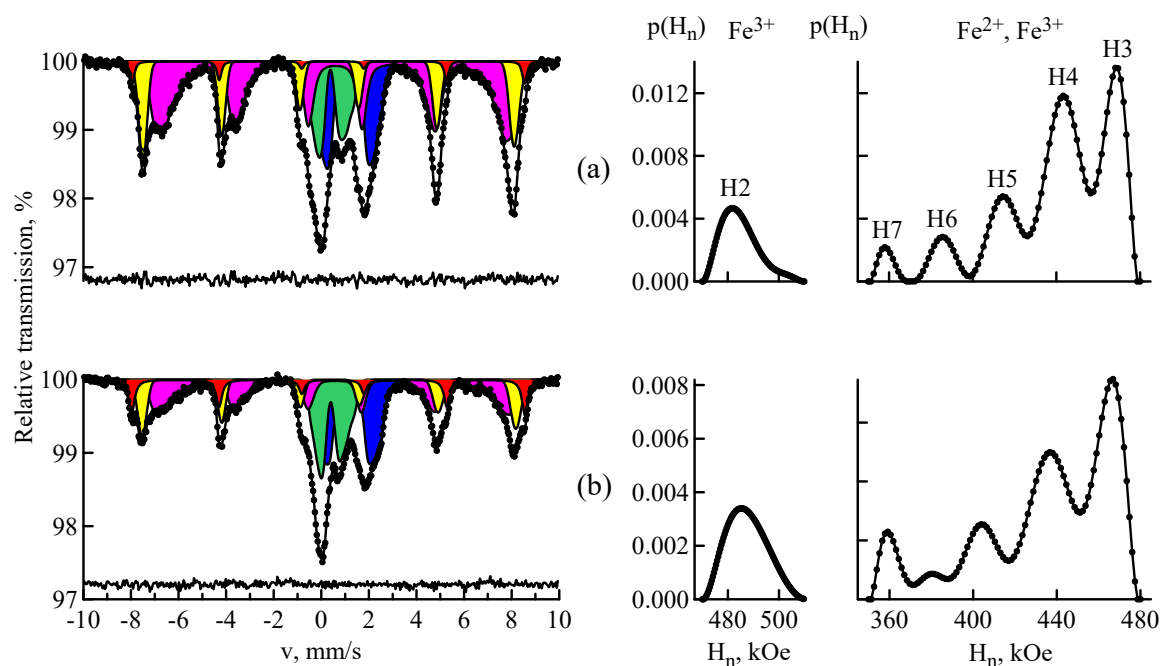
**Figure 2.** MS spectra of $^{57}$Fe nuclei in the samples of fly ashes FA1 (**a**) and FA2 (**b**); and restored distributions of hyperfine magnetic field p(H$_n$): hematite (red), magnetite (yellow and magenta), the paramagnetic minerals (blue and green).

**Table 1.** Hyperfine parameters of the magnetic fraction obtained from the MS spectrum of the fly ash FA1.

| Subspectrum | I, (%) | δ, mm/s | ε, mm/s | H$_n$, kOe | Assignment |
|:---:|:---:|:---:|:---:|:---:|:---:|
| H1 | 3.4 ± 0.8 | 0.39 ± 0.01 | −0.09 ± 0.01 | 512 ± 1 | Hematite |
| H2 | 19.9 ± 0.9 | 0.32 ± 0.01 | 0.01 ± 0.01 | 482 ± 1 | Magnetite [Fe$^{3+}$]$^{tetra}$ |
| H3 | 15.1 ± 0.9 | 0.55 ± 0.01 | 0.03 ± 0.01 | 468 ± 1 | Magnetite [Fe$^{3+}$]$^{octa}$ |
| H4 | 18.0 ± 0.9 | 0.57 ± 0.01 | 0.02 ± 0.01 | 443 ± 2 | Magnetite [Fe$^{2+}$]$^{octa}$ |
| H5 | 7.4 ± 0.4 | 0.60 ± 0.01 | 0.00 ± 0.01 | 414 ± 3 | Magnetite [Fe$^{2+}$]$^{octa}$ |
| H6 | 3.0 ± 0.4 | 0.63 ± 0.01 | 0.02 ± 0.01 | 385 ± 4 | Magnetite [Fe$^{2+}$]$^{octa}$ |
| H7 | 1.5 ± 0.3 | 0.66 ± 0.01 | 0.03 ± 0.01 | 358 ± 2 | Magnetite [Fe$^{2+}$]$^{octa}$ |

I: relative spectral area; δ: isomer shift relative to metallic iron at 300 K; ε: quadrupole shift; H$_n$: hyperfine field at $^{57}$Fe nuclei at maximum of the distribution.

The composition and properties of magnetite depend on conditions of its formation. This feature is associated with the fact that the isomorphic capacity of Fe$_3$O$_4$ is largely a function of temperature. At high temperatures, magnetite is able to capture impurities of several elements [23]. As a result of processing of the MS spectrum of the fly ash FA1, it has been established that the distribution of magnetic fields at $^{57}$Fe nuclei in the octahedral sublattice has several peaks. In addition, there is a correlation observed between the values of magnetic fields and corresponding isomer shifts. A smaller field corresponds to a larger isomer shift (see Table 1). The growth of impurity ion number in each of the nearest coordination shells around Fe atoms affects the magnetization and magnetic susceptibility. This leads to a change in the effective magnetic field at $^{57}$Fe nuclei–ΔH$_n$ [23,24]. The quite detailed explanation of the effect of substitutional impurities for certain elements on the values of the isomeric shift and hyperfine magnetic field is given in [25–27]. It is known [18,25] that the value of the isomeric shift depends on the degree of filling of s- and d-electron shells. Since the radius difference between the ground and excited states at $^{57}$Fe nuclei is negative, the isomeric shift increases with decreasing density and decreases with increasing density of external 4s-electrons. The dependence of the isomeric shift on the number of 3d-electrons, which screen 4s-electrons, is opposite. The value of the ΔH$_n$

contributions for the elements to the left of Fe in the periodic table of elements is negative and does not significantly depend on the nature of impurities. Thus, the isomer shift for $^{57}$Fe nuclei increases with the growth in the number of aluminum atoms in the nearest neighborhood of the iron atom [26]. This fact is explained by the transition of part of aluminum external electrons into the 3d-zone of iron.

Based on [23], magnetite formed at high temperature is capable of containing a number of isomorphic impurities (Al, Ti, Mg, Mn, Cr, Co, etc.). These impurities most often occupy the places in octahedral coordination, replacing $Fe^{2+}$ or $Fe^{3+}$. Aluminum mainly enters the octahedral coordination, replacing $Fe^{3+}$ ions. [23]. Titanium replaces $Fe^{2+}$ ions in the same coordination of magnetite [23]. Therefore, sextets H3-H7 with hyperfine fields of 358–468 kOe can be interpreted as a superposition of sextets, corresponding to $^{57}$Fe nuclei in the octa position of $Fe_3O_4$ with isomorphic impurities (Al and Ti).

The paramagnetic part of the spectrum of fly ash FA1 was fitted by two quadrupole shift distributions, separately for $Fe^{2+}$ and $Fe^{3+}$ ions with the relative spectral areas of 18.6% ± 0.7% and 13.1% ± 0.8%, respectively.

The spectrum of the ash FA2 was processed in the same model as the spectrum of FA1. Content of hematite α-$Fe_2O_3$ (sextet H1) in the fly ash FA2 was significantly higher than in the fly ash FA1. As in the case of the fly ash FA1, the sextet H2 was assigned to the ions $Fe^{3+}$ in the tetrahedral position of magnetite $Fe_3O_4$. The sextets H3 and H4–H7 were specified by unequal positions of $Fe^{3+}$ and $Fe^{2+}$ ions respectively in the octahedral position. As it can be noted from Figure 2, distribution of hyperfine magnetic fields in the tetrahedral sublattice of the magnetite of ash FA2 was broader compared to the similar distribution of ash FA1. Since S(A)/S(B) = 0.62 ± 0.09, it should be assumed that the sextet H2 was complemented by the contribution due to foreign iron-containing impurities. It should be considered that such an impurity is a maghemite γ-$Fe_2O_3$. Maghemite, like magnetite, has a reversed spinel structure; therefore, its MS spectrum contains two sextets due to $Fe^{3+}$ ions in the tetrahedral position in the A-sublattice and $Fe^{3+}$ in the octahedral position in the B-sublattice [28,29]. Owing to the fact that the values of hyperfine parameters from $Fe^{3+}$ ions in the A- and B-sublattice are close in value, the spectrum of γ-$Fe_2O_3$ is often interpreted as one sextet [11,13]. Considering above, the spectrum of the ash FA2 was processed according to the model that contained the added two sextets with the Mössbauer parameters of maghemite [28]. Fitting of the spectrum of the fly ash FA2 (Figure 3) showed that the magnetic part of the spectrum was best described by four sextets and one distribution of $^{57}$Fe hyperfine magnetic fields in the interval of 350–480 kOe. The parameters and interpretation of the magnetic part of the spectrum for the ash FA2 are provided in Table 2. S(A)/S(B) = 0.36 ± 0.09, which corresponded to the population of $Fe^{3+}$ ions in the A- and B-positions of magnetite. In this case, the described above hypothesis on the presence of certain magnetically ordered phase in the fly ash was considered. It should be noted that the magnetic fields at $^{57}$Fe nuclei in α-$Fe_2O_3$, γ-$Fe_2O_3$ and $Fe_3O_4$ had lower values compared with those for the well-crystallized minerals. This is typical of the finely dispersed magnetic materials.
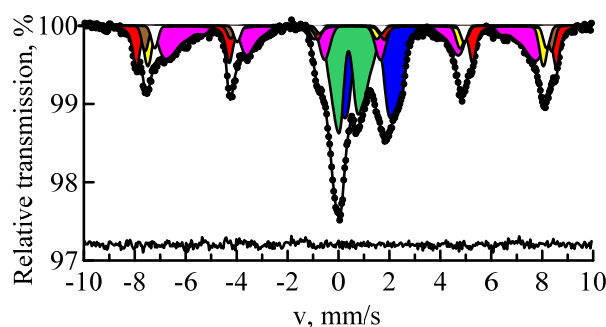


**Figure 3.** MS spectrum of $^{57}$Fe nuclei in the sample of fly ash FA2: hematite (red); maghemite (brown and white); magnetite (yellow and magenta) and the paramagnetic minerals (blue and green).

The paramagnetic part of the spectrum of the fly ash FA2, as well as FA1, is represented by two quadrupole shifts distributions, separately for $Fe^{2+}$ and $Fe^{3+}$ ions with relative spectral areas of $25.7\% \pm 0.9\%$ and $20.2\% \pm 0.9\%$, respectively.

**Table 2.** Hyperfine parameters of the magnetic fraction obtained from the MS spectrum of the fly ash FA2.

| Subspectrum | I, (%) | $\delta$, mm/s | $\varepsilon$, mm/s | $H_n$, kOe | Assignment |
|---|---|---|---|---|---|
| H1 | $13.7 \pm 0.9$ | $0.34 \pm 0.01$ | $-0.09 \pm 0.01$ | $512 \pm 1$ | Hematite |
| M1 | $4.2 \pm 0.9$ | $0.39 \pm 0.01$ | $0.00 \pm 0.01$ | $495 \pm 1$ | Maghemite $[Fe^{3+}]^{tetra}$ |
| M2 | $4.4 \pm 0.2$ | $0.48 \pm 0.02$ | $0.00 \pm 0.01$ | $477 \pm 2$ | Maghemite $[Fe^{3+}]^{octa}$ |
| H2 | $8.2 \pm 0.9$ | $0.28 \pm 0.02$ | $0.00 \pm 0.01$ | $482 \pm 1$ | Magnetite $[Fe^{3+}]^{tetra}$ |
| H3 | $10.0 \pm 0.9$ | $0.52 \pm 0.01$ | $0.03 \pm 0.01$ | $458 \pm 4$ | Magnetite $[Fe^{3+}]^{octa}$ |
| H4 | $6.8 \pm 0.9$ | $0.53 \pm 0.01$ | $0.02 \pm 0.01$ | $434 \pm 5$ | Magnetite $[Fe^{2+}]^{octa}$ |
| H5 | $4.6 \pm 0.5$ | $0.54 \pm 0.01$ | $0.02 \pm 0.01$ | $402 \pm 5$ | Magnetite $[Fe^{2+}]^{octa}$ |
| H6 | $2.2 \pm 0.4$ | $0.55 \pm 0.01$ | $0.00 \pm 0.01$ | $359 \pm 2$ | Magnetite $[Fe^{2+}]^{octa}$ |

The samples of the ashes FA1 and FA2, subjected to magnetic separation, were studied for interpretation of the paramagnetic part. As it was mentioned in the Introduction the non-magnetic part of fly ashes contains minerals such as hercynite and mullite. Hercynite is a ferrous mineral with the structure of normal spinel, a paramagnet with cubic syngony, general formula is $FeAl_2O_4$. The theoretical composition of hercynite is FeO—41.34% and $Al_2O_3$—58.66% [30]. Often Fe is isomorphically replaced by Mg, sometimes by Mn; Al is replaced by Fe and Cr. Based on the structural type of normal spinel, the bivalent cations ($Fe^{2+}$) are surrounded by four oxygen ions in tetrahedral coordination; while the trivalent cations ($Al^{3+}$, $Fe^{3+}$) are surrounded by six oxygen ions at the vertices of the octahedra. It should be noted that each ion of oxygen is associated with one bivalent and three trivalent cations. The structure of hercynite is characterized by a combination of isometric tetrahedra and octahedra in such a way that each vertex is common for one tetrahedron and three octahedra [31]. The structural formula of this mineral can be represented as follows: $[Fe^{2+} IV]^{tetra}[Fe^{2+} VI (Al^{3+} VI)]^{octa}$. The symbols IV and VI correspond to tetra and octa coordination, respectively.

Mullite is one of the main components of fly ash and the only mineral from the aluminosilicate family that is stable at high temperature ($T_{melt}$ = 1810–1830 °C) [32]. It belongs to the most important technical materials and therefore is the subject of numerous studies, which are summarized in the review [33]. Mullite has a variable composition, ranging from $3Al_2O_3 \cdot 2SiO_2$ to $2Al_2O_3 \cdot SiO_2$. Its structure is rhombic. According to the authors of [34], mullite is a chain silicate rich in aluminum. Aluminum ions can be contained in the lattice with a coordination number 6 and 4, appearing both in the octahedral and tetrahedral positions. The structural formula of mullite can be written as follows $[4Al^{3+} VI]^{octa} [Al^{3+} IV (Si_2^{4+} IV)]^{tetra} O_{13}$. Mullite is able to form the solid solutions with various oxides [35]. The substitutional solid solution is formed when $Fe_2O_3$ is added. In this case, the $Fe^{3+}$ ions replace the $Si^{4+}$ ions in octahedral and tetrahedral positions. When FeO is added, the $Fe^{2+}$ ions can replace the $Si^{4+}$ ions in the tetrahedral position, but the probability of such chemical transformation is low [36,37]. In mullite, isovalent and heterovalent isomorphism is observed. According to Goldschmidt's law [38], if the crystal lattice has vacant sites, then charge for heterovalent isomorphism is compensated by additional ions. As a result, one ion of higher valence is replaced by two ions of lower valence. It should be expected that iron in mullite due to isomorphic substitution can appear in at least three non-equivalent positions: $(Fe^{3+} \rightarrow Al^{3+})^{octa}$, $(Fe^{3+} \rightarrow Al^{3+})^{tetra}$, $(Fe^{2+} \rightarrow Si^{4+})^{tetra}$. Partial isomorphic substitution of $Al^{3+}$ by $Fe^{3+}$ in the lattices of hercynite and mullite occurs due to proximity of the ionic radii of $Al^{3+}$ and $Fe^{3+}$ (0.57 and 0.67 Å respectively).

Considering above, the MS spectra of fly ashes FA1 and FA2 after magnetic separation (Figure 4) were processed with sufficient quality using two groups of doublets. The first group consists of three doublets, characterizing the $Fe^{2+}$ ions in the tetrahedral and the $Fe^{2+}$, $Fe^{3+}$ ions in the octahedral environment in the crystal lattice of hercynite. The parameters of these doublets are similar to the

parameters of hercynite produced by the arc-melting method under the protective argon atmosphere [39]. The second group also consists of three doublets, defined by $Fe^{3+}$ ions in the octahedral $Fe^{3+}$, $Fe^{2+}$ in the tetrahedral environment and in the crystal lattice of mullite. In addition, the spectrum contains a doublet related to $Fe^{2+}$ in the octahedral environment of silicate glass [11,14]. The parameters of doublets describing the non-magnetic fraction of the fly ashes FA1 and FA2 are provided in Table 3.
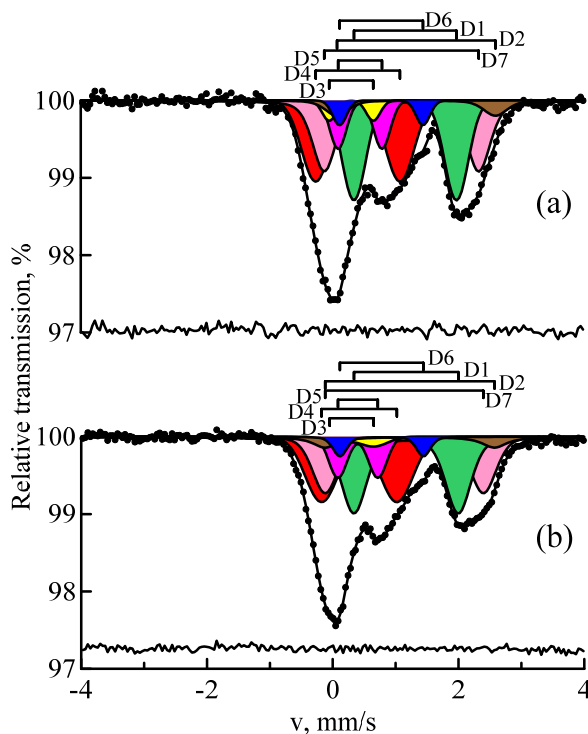


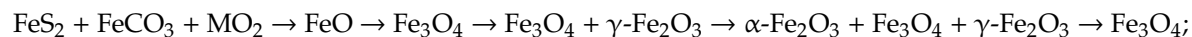**Figure 4.** MS spectra of $^{57}$Fe nuclei in the samples of the non-magnetic fraction of fly ashes FA1 (**a**) and FA2 (**b**).

**Table 3.** Hyperfine parameters of the non-magnetic fraction of the fly ashes FA1 and FA2.

| Sample | Subspectrum | I, (%) | $\delta$, mm/s | $\varepsilon$, mm/s | Assignment |
|--------|-------------|--------|---------|---------|------------|
| FA1 | D1 | 27.7 ± 0.9 | 1.16 ± 0.01 | 0.82 ± 0.01 | Hercynite [$Fe^{2+}$]$^{tetra}$ |
| | D2 | 5.0 ± 0.1 | 1.33 ± 0.04 | 1.26 ± 0.03 | Hercynite [$Fe^{2+}$]$^{octa}$ |
| | D3 | 3.3 ± 0.2 | 0.30 ± 0.09 | 0.35 ± 0.09 | Hercynite [$Fe^{3+}$]$^{octa}$ |
| | D4 | 27.0 ± 0.7 | 0.41 ± 0.05 | 0.67 ± 0.09 | Mullite [$Fe^{3+}$]$^{octa}$ |
| | D5 | 9.4 ± 0.1 | 0.44 ± 0.09 | 0.35 ± 0.08 | Mullite [$Fe^{3+}$]$^{tetra}$ |
| | D6 | 4.1 ± 0.3 | 0.78 ± 0.05 | 0.66 ± 0.05 | Mullite [$Fe^{2+}$]$^{tetra}$ |
| | D7 | 23.5 ± 0.9 | 1.10 ± 0.01 | 1.23 ± 0.01 | Silicate [$Fe^{2+}$]$^{octa}$ |
| FA2 | D1 | 29.2 ± 0.9 | 1.17 ± 0.01 | 0.83 ± 0.01 | Hercynite [$Fe^{2+}$]$^{tetra}$ |
| | D2 | 5.2 ± 0.1 | 1.35 ± 0.04 | 1.26 ± 0.03 | Hercynite [$Fe^{2+}$]$^{octa}$ |
| | D3 | 3.5 ± 0.2 | 0.30 ± 0.09 | 0.35 ± 0.09 | Hercynite [$Fe^{3+}$]$^{octa}$ |
| | D4 | 27.4 ± 0.9 | 0.42 ± 0.05 | 0.60 ± 0.09 | Mullite [$Fe^{3+}$]$^{octa}$ |
| | D5 | 9.6 ± 0.1 | 0.40 ± 0.09 | 0.32 ± 0.08 | Mullite [$Fe^{3+}$]$^{tetra}$ |
| | D6 | 4.1 ± 0.1 | 0.78 ± 0.05 | 0.66 ± 0.05 | Mullite [$Fe^{2+}$]$^{tetra}$ |
| | D7 | 21.0 ± 0.9 | 1.14 ± 0.01 | 1.26 ± 0.01 | Silicate [$Fe^{2+}$]$^{octa}$ |

Thus, the spectra of the fly ashes FA1 and FA2 are generally similar but differ in two important aspects. The amount of hematite $\alpha$-$Fe_2O_3$ was almost 4 times more in the ash FA2. It is known [13,16] that magnetite is a more stable oxide at high temperatures, while hematite is more stable at T < 1388 °C. To confirm this fact, coal was burned at the temperature of 800–900 °C [40]. It turned out that

magnetically ordered iron was predominantly in the form of $\alpha$-$Fe_2O_3$ in the composition of the fly ash, iron in the form of $Fe_3O_4$ was also present, but in a much smaller amount.

$FeS_2$ and $FeCO_3$ decayed when coal was burned in the Ekibastuz basin at T $\approx$ 500 °C. There was a gradual increase of the oxidation state of iron: first, formation of FeO, then $Fe_3O_4$ and finally, $\alpha$-$Fe_2O_3$ through the intermediate $\gamma$-$Fe_2O_3$ phase. Oxidation to higher oxide continued to the temperature of T = 1388 °C. At T $\geq$ 1400 °C $\alpha$-$Fe_2O_3$ was converted to $Fe_3O_4$ in carbon atmosphere. Formation of magnetically ordered minerals in the furnace unit can be represented as follows:

$$FeS_2 + FeCO_3 + MO_2 \rightarrow FeO \rightarrow Fe_3O_4 \rightarrow Fe_3O_4 + \gamma\text{-}Fe_2O_3 \rightarrow \alpha\text{-}Fe_2O_3 + Fe_3O_4 + \gamma\text{-}Fe_2O_3 \rightarrow Fe_3O_4;$$

where M is the amount of $O_2$, depending on the operation mode of the furnace unit.

Two competing processes can occur while burning coal: the reactions of thermo-chemical transformation in the reducing carbon atmosphere and the reactions occurring in the oxidizing atmosphere. As a result, the mineral components of coal being located in the flare flame (3–5 s) at the temperature of 1400–1900 °C turn into fly ash. It is well known from the reactions, occurring in the blast furnace [41], that a mixture of oxide CO and carbon dioxide $CO_2$ reduces ore to metallic iron. This happens when the $CO_2/CO$ ratio is maintained below a certain value, which depends on the temperature. If this value is higher, the iron will oxidize. In normal combustion of coal, a gas mixture was formed, which contained sufficient $CO_2$ to oxidize the iron. In contrast to the authors of [42], no signs of pure iron presence were found in this study, i.e., no traces of the reducing atmosphere were detected. This gives the right to assert that the processes occur in the oxidizing atmosphere.

According to the results of chemical analysis, the content of iron oxides in the fly ash of the Ekibastuz coal was 5.56%. Chemical analysis of elemental composition of fly ashes was carried out by the X-ray fluorescence method. The obtained iron content (5.56%) is close to the value indicated in [4]. Therefore, the amount of iron, localized in the magnetically ordered and paramagnetic matrix, was determined from the relative areas of certain components of the Mössbauer spectra, and then the iron content was calculated in certain components of the studied samples (Table 4). Table 4 shows that iron was concentrated mainly in the structure of magnetite in the fly ash FA1. Maghemite was present only in the fly ash FA2. The lower content of hercynite in fly ash FA1 could be explained by the fact that at high temperatures it decomposed with the formation of magnetite. Indeed, hercynite was present in the fly ash in the form of oriented intergrowths with magnetite. Above 858 °C, the mutual solubility of $FeAl_2O_4$ and $FeFe_2O_4$ was unlimited [31]. In addition, this mineral melted incongruently (with decomposition) at T = 1440 °C. At T = 1300 °C, the maximum content of iron (10%) was reached in mullite, but at T = 1400 °C its content decreased (to 6.5%) [33,36]. Thus, at high temperatures due to decay of hematite, maghemite and hercynite and a decrease in the amount of iron in mullite, the fraction of magnetite increased in the fly ash FA1. Consequently, the analysis of the fly ash phase composition enabled us to make the conclusion that the amount of iron, contained in magnetite, was a temperature indicator of fly ashes formation.

**Table 4.** Content of iron oxides (%) in the samples of fly ashes FA1 and FA2.

| Sample | Hematite | Maghemite | Magnetite | Hercynite | Mullite | Silicate |
|--------|----------|-----------|-----------|-----------|---------|----------|
| FA1 | 0.19 | - | 3.61 | 0.63 | 0.71 | 0.37 |
| FA2 | 0.76 | 0.48 | 1.77 | 0.97 | 1.05 | 0.54 |

Error is not above 0.04.

### 3.2. X-ray Diffraction

The use of the X-ray diffraction method complements the information on the phase composition of the studied materials [42,43]. Figure 5 shows X-ray diffraction patterns of the samples FA1 and FA2. Against the background of halo, indicating the presence of the amorphous phase, the reflections of quartz $SiO_2$ (Q) and mullite $Al_6Si_2O_{13}$ (Mu) were confidently identified. In addition, there were the

reflections of magnetite $Fe_3O_4$ (Mg), maghemite $\gamma$-$Fe_2O_3$ (Mh), hematite $\alpha$-$Fe_2O_3$ (Hm) and hercynite $FeAl_2O_4$ (He). Differentiation of the reflections responsible for $Fe_3O_4$ and $\gamma$-$Fe_2O_3$ was difficult since the diffraction peaks in the X-ray images were overlapping. The reflections of maghemite $\gamma$-$Fe_2O_3$ (Mg) were more visible in the X-ray image of the fly ash FA2, which agreed quite well with the Mössbauer results. In addition to the indicated phases, the reflections, close to the reflections of calcite $CaCO_3$ (Ca), were observed in the X-ray image of the fly ash FA2. Calcite is the most stable of the three modifications of calcium carbonate. During annealing at the temperatures above 1500 °C in the atmosphere of carbon excess pressure, it is transferred to calcium carbide $CaC_2$ [44]. However, there are no characteristic reflections of this mineral in the X-ray diffraction pattern of the sample FA1.
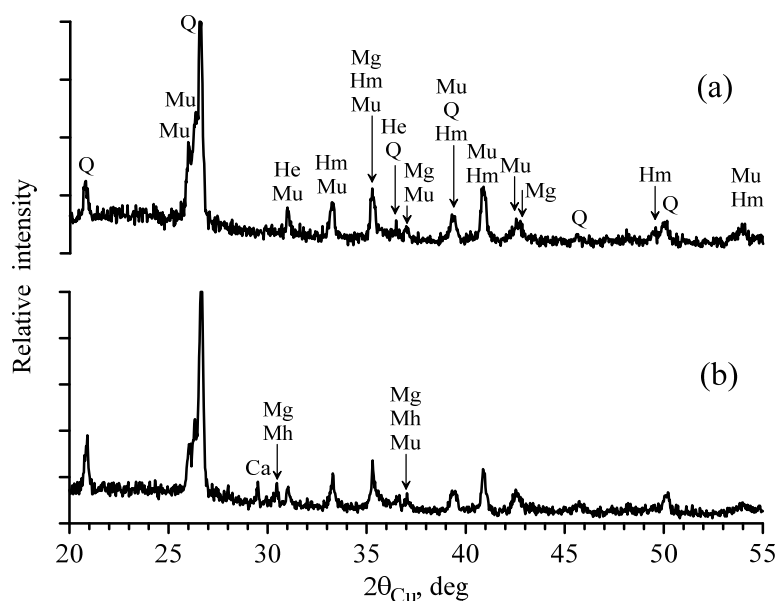


**Figure 5.** XRD patterns of the fly ashes samples FA1 (**a**) and FA2 (**b**).

## 4. Conclusions

Mössbauer spectroscopy was used to study samples of fly ashes formed after the combustion of coal from the Ekibastuz basin at the thermal power plants TPP-2 and TPP-3 in Almaty. It was established that the fractions of fly ashes contained iron in the form of magnetite $Fe_3O_4$ and hematite $\alpha$-$Fe_2O_3$. The mixed valence of iron $Fe^{3+} \leftrightarrow Fe^{2+}$ in the octahedral sublattice of magnetite was destroyed by isostructural substitution impurities. Maghemite $\gamma$-$Fe_2O_3$ was additionally present in the fly ash of TPP-3 as a product of magnetite slow oxidation. It was shown that at T $\geq$ 1400 °C, the proportion of magnetite increased in fly ash due to decay of hematite, maghemite, hercynite and a decrease in the iron content in mullite. It was concluded that the amount of iron in magnetite was a temperature indicator of fly ashes formation. The parameters of hyperfine interactions were determined in the iron-containing minerals of fly ash. It was identified that formation of the fly ashes structure occurred in the oxidizing atmosphere, since no traces were revealed of reducing environment effect on the phase composition.

The X-ray diffraction method revealed the amorphous state of minerals, quartz, mullite and calcite. In addition, there were the reflections of magnetite, maghemite, hematite $\alpha$-$Fe_2O_3$ and hercynite.

## References

1.  Kizilshtein, L.Y. Traces of coal-fired power industry. *Sci. Life* **2008**, *5*, 42–47.
2.  Samorokov, V.E.; Zelinskaya, E.V. Use of micro-spheres in composite materials. *Bull. Irkutsk State Univ.* **2012**, *9*, 201–205.
3.  Zorya, V.N.; Korovushkinm, V.V.; Permyakov, A.A.; Volynkina, E.P. The research of the mineral composition and crystal structure of iron-containing components of technogenic waste of the metallurgical complex. *Izvestiya. Ferrous Metall.* **2015**, *58*, 359–366. [CrossRef]
4.  Adeeva, L.N.; Borbat, V.F. Heating and power plant ash—The promising raw materials for the industry. *Bull. Omsk Univ.* **2009**, *2*, 141–151.
5.  Harchand, K.S.; Taneja, S.P.; Raj, D.; Sharma, P. Mössbauer studies of coal ash. *Fuel Process. Technol.* **1989**, *21*, 19–24. [CrossRef]
6.  Liu, L.; Peng, B.; Yue, C.; Guo, M.; Zhan, M. Low-cost, shape-stabilized fly ash composite phase change material synthesized by using a facile process for building energy efficiency. *Mater. Chem. Phys.* **2019**, *22215*, 87–95. [CrossRef]
7.  Zyryanov, V.V.; Petrov, S.A.; Matvienko, A.A. Characterization of spinel and magnetospheres of coal fly ashes collected in power plants in the former USSR. *Fuel* **2011**, *90*, 486–492. [CrossRef]
8.  Kizilshtein, L.; Dubov, I.; Shpitsgluz, A.; Parada, S. *Components of Ashes and Slags of Heat Power Plants*; Energoatomizdat: Moscow, Russia, 1995.
9.  Sharonova, O.M.; Anshits, N.N.; Solovyov, L.A.; Salanov, A.N.; Anshits, A.G. Relationship between composition and structure of globules in narrow fractions of ferrospheres. *Fuel* **2013**, *111*, 332–343. [CrossRef]
10. Sokol, E.V.; Kalugin, V.M.; Nigmatulina, E.N.; Volkova, N.I.; Maksimova, N.V. Ferrospheres from fly ashes of Chelyabinsk coals: Chemical composition, morphology and formation conditions. *Fuel* **2002**, *81*, 867–876. [CrossRef]
11. Yang, J.; Zhao, Y.; Zyryanov, V.; Zhang, J.; Zhenga, C. Physical–chemical characteristics and elements enrichment of magnetospheres from coal fly ashes. *Fuel* **2014**, *135*, 15–26. [CrossRef]
12. Anshits, N.N.; Solov'ev, L.A.; Rabchevskii, E.V.; Anshits, A.G.; Bayukov, O.A.; Eremin, E.V. Mössbauer and magnetic investigations of high-iron samples of energy ashes. *Phys. Solid State* **2010**, *52*, 1188–1192. [CrossRef]
13. Vandenberghe, R.E.; de Resende, V.G.; da Costa, G.M.; Grave, E. De Study of loss-on-ignition anomalies found in ashes from combustion of iron-rich coal. *Fuel* **2010**, *89*, 2405–2410. [CrossRef]
14. Hinckley, C.C.; Smith, G.V.; Twardowska, H.; Saporoschenko, M.; Shiley, R.H.; Griffen, R.A. Mossbauer studies of iron in Lurgi gasification ashes and power plant fly and bottom ash. *Fuel* **1980**, *59*, 161–165. [CrossRef]
15. Harchand, K.S.; Raj, D. Characterization of iron-bearing phases in coal and their ash. *Nucl. Instrum. Methods Phys. Res. Sect. B: Beam Interact. Mater. At.* **1993**, *76*, 249–251. [CrossRef]
16. Patil, M.D.; Eaton, H.C.; Tittlebaum, M.E. [57]Fe Mössbauer spectroscopic studies of fly ash from coal-fired power plants and bottom ash from lignite-natural gas combustion. *Fuel* **1984**, *63*, 788–792. [CrossRef]
17. Matsnev, M.E.; Rusakov, V.S. SpectrRelax: An application for Mössbauer spectra modeling and fitting. *AIP Conf. Proc.* **2012**, *1489*, 178–185.
18. Goldanskii, V.; Herber, R. *Chemical Applications of Mössbauer Spectroscopy*; Academic: New York, NY, USA, 1968.
19. Kadyrzhanov, K.K.; Vereshchak, M.F.; Manakova, I.A.; Ozernoy, A.N.; Rusakov, V.S. Structure-phase transformations in the Be-Fe-Be layered system subjected to irradiation and thermal treatment. *J. Phys. Chem. Solids* **2013**, *74*, 1078–1085. [CrossRef]
20. Ozernoy, A.N.; Vereshchak, M.F.; Manakova, I.A.; Tleubergenov, Z.K.; Bedelbekova, K.A. Nuclear gamma-resonance spectroscopy in study of nanoscale composites. *Phys. At. Nucl.* **2018**, *81*, 1484–1487. [CrossRef]

21. Donbaev, K.M.; Zhetbaev, A.K.; Mukusheva, M.K.; Donbaeva, V.A. Mössbauer investigations of single crystal hematite doped with impurities. *Phys. Status Solidi* **1994**, *143*, K41–K44. [CrossRef]

22. Shipilin, M.A.; Zakharova, I.N.; Shipilin, A.M.; Bachurin, V.I. Mossbauer studies of magnetite nanoparticles. *J. Surf. Investig. X-Ray Synchrotron Neutron Tech.* **2014**, *8*, 357–361. [CrossRef]

23. Chernysheva, N.; Smelyanskaya, G.; Zaitseva, G. *Typomorphism of Magnetite and Its Use in Search for and Assesment of Ore Deposits*; Nedra: Moscow, Russia, 1981.

24. Manakova, I.A.; Vereshchak, M.F.; Sergeeva, L.S.; Shokanov, A.K.; Antonyuk, V.I.; Rusakov, V.S.; Kadyrzhanov, K.K. Laws of thermally induced formation of phases in $\alpha$-Fe with a titanium coating upon isochronous annealings. *Phys. Met. Metallogr.* **2010**, *109*, 447–460. [CrossRef]

25. Ovchinnikov, V. *Mössbauer Methods for Analysis of Atomic and Magnetic Structure of Alloys*; Fizmatlit: Moscow, Russia, 2002.

26. Litvinov, V.; Karakishev, S.; Ovchinnikov, V. *Nuclear $\gamma$-Resonance Spectroscopy of Alloys*; Metallurgiya: Moscow, Russia, 1982.

27. Sagaradze, V.V.; Shabashov, V.A.; Mukoseev, A.G.; Pecherkina, N.L.; Sagaradze, I.V. Dissolution of Carbon-Containing Particles such as Soot, Cementite, and VC Carbides in FCC Fe-Ni Alloys upon Severe Cold Deformation. *Phys. Met. Metallogr.* **2001**, *91*, 299–307.

28. Zakharova, I.N.; Shipilin, M.A.; Alekseev, V.P.; Shipilin, A.M. Mössbauer study of maghemite nanoparticles. *Tech. Phys. Lett.* **2012**, *38*, 55–58. [CrossRef]

29. Kamzin, A.S.; Valiullin, A.A.; Khurshid, H.; Nemati, Z.; Srikanth, H.; Phan, M.H. Mössbauer Studies of Core-Shell FeO/Fe$_3$O$_4$ Nanoparticles. *Phys. Solid State* **2018**, *60*, 382–389. [CrossRef]

30. Larsson, L.; O'Neill, H.S.C.; Anncrsten, H. Crystal chemistry of synthetic hercynite (FeAl$_2$0$_4$) from XRD structural refinements and Mössbauer spectroscopy. *Eur. J. Mineral.* **1994**, *6*, 39–51. [CrossRef]

31. Chukhrov, F.; Bonshtedt-Kupletskaya, É. *Minerals. Compound Oxides, Titanates, Niobates, Antimonates, and Hydroxides (Handbook)*; Nauka: Moscow, Russia, 1967.

32. Fomenko, E.V.; Anshits, N.N.; Vasil'eva, N.G.; Rogovenko, E.S.; Mikhaylova, O.A.; Mazurova, E.V.; Solov'ev, L.A.; Anshits, A.G. Composition and structure of the shells of aluminosilicate microspheres in fly ash formed on the combustion of Ekibastuz coal. *Solid Fuel Chem.* **2016**, *50*, 238–247. [CrossRef]

33. Yarotskaya, E.G.; Fedorov, P.P. Mullite and its isomorphic substitutions. Overview. *Condens. Matter Interphases* **2018**, *20*, 537–544.

34. Gorshkov, V.; Savelyev, V.; Fedorov, N. *Physical Chemistry of Silicates and other Refractory Compounds*; Vysshaya Shkola Publishing: Moscow, Russia, 1988.

35. Pimkov, Y. Synthesis of Mullite from Activated Precursors and Composite Materials Based on It. Ph.D. Dissertation, Ivanovo State University of Chemistry and Technology, Ivanovo, Russia, 2016.

36. Urusov, V. *Theory of Isomorphic Mixability*; Nauka: Moscow, Russia, 1977.

37. Makarov, E. *Isomorphism of Atoms in Crystals*; Atomizdat: Moscow, Russia, 1973.

38. Goldschmidt, V. *Kristallchemie*; Verlag von Gustav Fischer: Jena, Germany, 1934.

39. Jastrzębska, I.; Szczerba, J.; Stoch, P.; Błachowski, A.; Ruebenbauer, K.; Prorok, R.; Snieżek, E. Crystal structure and Mössbauer study of FeAl$_2$O$_4$. *Nukleonika* **2015**, *60*, 47–49. [CrossRef]

40. Vereshchak, M.F.; Manakova, I.A.; Shokanov, A.K. Mössbauer research of minerals contained in coals of Kazakhstan. *NNC RK Bull.* **2019**, *4*, 13–16.

41. Sibagatullin, S.K.; Kharchenko, A.S.; Polinov, A.A.; Pavlov, A.V.; Semenyuk, M.A.; Beginyuk, V.A. Stabilization of the ratio of natural gas and blast flows through blast furnace tuyeres. *Theory Technol. Metall. Prod.* **2014**, *1*, 23–25.

42. Bhattacharjee, A.; Mandal, H.; Roy, M.; Kusz, J.; Hofmeister, W. Microstructural and magnetic characterization of fly ash from Kolaghat Thermal Power Plant in West Bengal, India. *J. Magn. Magn. Mater.* **2011**, *323*, 3007–3012. [CrossRef]

43. Taneja, S.P.; Harchand, K.S.; Raj, D.; Chandra, K. Characterization of iron phases in coal ash from thermal power plant. *Fuel Process. Technol.* **1991**, *29*, 209–217. [CrossRef]

44. Volkov, A.; Zharsky, I. *Great Chemical Reference*; Modern School: Minsk, Belarus, 2005.